Hyperspectral Imaging Analysis of Simulated Scenes for Space Domain Awareness

Felicitas Hernandez, Scott Almond, and Max Li
Northrop Grumman

1. ABSTRACT

Space-based hyperspectral sensing presents a novel application of optical sensor technology to intelligence gathering of unique characteristics of man-made objects which cannot be obtained by current conventional means. Supported by advancements in machine learning, these complex multi-dimensional data sets can be distilled into a manageable collection of actionable parameters useful for applications such as spoofing recognition and non-resolvable object identification. This paper presents the development of a photons-to-knowledge algorithm pipeline that simulates end-to-end sensor performance. With reliable real-world data inputs, this model performance assessment informs a wide range of design trades which both supplements and elucidates the capabilities of the physical hardware sensor.

This paper focuses primarily on the development of a synthetic scene generator and machine learning classifier. A parameter sensitivity assessment is performed, and findings are presented, in a variety of use cases, target compositions, and sensor configurations. Recommendations are provided for metrics of interest to frame the discussion about hyperspectral space domain awareness sensor performance. By using the knowledge from this algorithm package, an extension of this simulation to real-world sensors and data can then efficiently allow for the analysis of unique target characteristics.

2. INTRODUCTION

Space-based infrastructure is an integral part of a diverse collection of critical technologies including communications, weather forecasting, and navigation. As our reliance on these technologies continues to grow, Space Domain Awareness (SDA)—the ability to detect, monitor, and characterize space objects—provides essential information for mitigating risks to space-based assets [1-5]. Although substantial investment in ground-based SDA technologies has resulted in promising advances, space-based SDA systems allow for elimination of coverage gaps [1-5], improved performance due to atmosphere-free observing conditions, proximity to targets of interest, diversity of observation geometry, and improved reaction time, all of which result in a greater degree of fidelity and enhanced risk protection.

The US began space-based space surveillance in 1996 with the Space-Based Visible (SBV) instrument on the Midcourse Space Experiment (MSX) bus. This mission thread was continued in sun-synchronous LEO with Space Based Space Surveillance (SBSS), XSS, Micro-Satellite Technology Experiment (MITEx), STARE, and Operationally Responsive Space (ORS)-5, and more recently with Geosynchronous Space Situational Awareness Program (GSSAP) in a near-GEO orbit. These instruments leverage panchromatic sensing elements [1-5], which are limited to analyzing targets based on time-varying light curves and orbital analysis and thus provide only limited utility of intelligence. In adjacent science domains (climate, weather, earth resource detection), sensors have exploited numerous spectral bands to improve identification and the quality of data products [6-16]. Given the chaos of a spectrally indiscriminate scene, we use our knowledge of the phenomenology of the source, illuminator, and atmosphere to refine our knowledge of perceived phenomena—the fundamental rule being the more bands available in high SNR scenes, the better we are able to understand a source or region of interest.

Extension of this rule leads to the concept of Hyperspectral Imaging (HSI), which functions similarly to traditional cameras while also capturing a target's spectral signature over a large number of spectral bins. This enables unique capabilities for SDA by revealing new information about the material composition such as country of origin, age of materials, continuous custody, closely spaced objects, thruster gas plume composition, and physical temperature (Fig. 1). Artificial intelligence and machine learning (AI/ML) analysis revealing this information will extend the range of applications available to space-based imaging systems, as well as improving the fidelity and decision-making paradigms for existing systems.

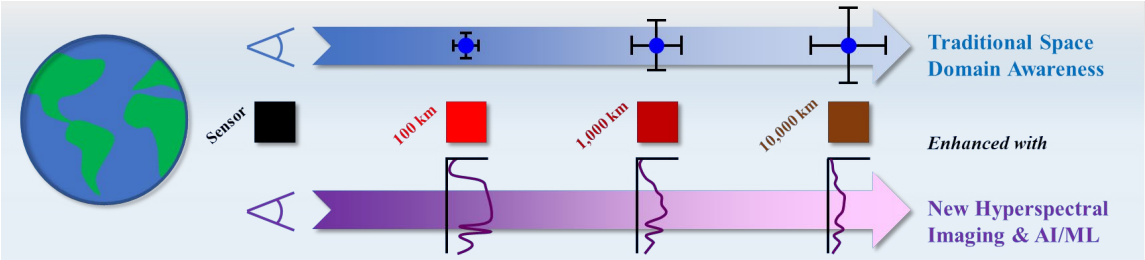

Fig. 1. Mission Application Overview

Past work utilizing HSI has been primarily for Earth-viewing missions *(e.g.* Indian Pines, Pavia University, Kennedy Space Center) [6-16]. Unmanned aerial vehicle (UAV) imaging of localized ground scenes have been used for landscape and mineral analysis, while space-based missions typically leverage LEO to achieve optimal spatial resolution versus globe coverage [6-16]. This previous work has shown classification of different landscape features (soil, rock, and different types of crops) with accuracies >90% [6-16]. Due to the application space of these Earth-viewing missions, to achieve tight spatial resolution (~10m pixels) push-broom architectures and high frame rates (>100 Hz) are the norm with brief (milliseconds) views of the scene, low along-track spatial resolution (>100 urad), and low cross-track field-of-view (FOV) (<100 mrad), predominantly limiting these architectures to day-time operation. However, these properties are insufficient for SDA applications, in which a plethora of targets may be observed at long distances with a diversity of size, form factors, material composition, CONOPs, and lighting conditions. These diverse aspects of HSI-based SDA present challenges to hardware design and data processing across systems favoring <10 urad resolution, FOVs of multiple degrees, long (seconds) duration captures, and comparatively dark scenes resulting in increased importance on preserving photon throughputs. In particular, low data downlink volumes and long viewing distances to targets result in a dearth of data for analysis, while the large design space results in complicated, lengthy and expensive hardware development.

This paper targets addressing these issues by demonstrating a three-part end-to-end photons-to-knowledge math model simulator and information extractor consisting of a synthetic scene generator (SSG), pre-processing algorithms, and machine learning (AI/ML) classifier. The simulator aims to utilize the flexibility, speed, and low cost of software (compared to hardware systems) to both generate large volumes of synthetic data for analysis while allowing for a broader examination of the entire HSI-SDA design space by freely tuning architectural parameters. Generation and analysis of reasonably realistic data informed by real-world spectra will enable insight into the overall system performance for previously unexplored SDA GEO applications.

3. MATH MODEL OVERVIEW

An overview of the math model is provided in Fig. 2. Real-world data is used to inform a tunable synthetic scene generator (SSG) also based on real-world optical architectures. Scenes generated from the SSG are passed to pre-processing algorithms for target extraction and normalization for AI/ML training and testing for performance assessment (*e.g.* classification accuracy). For the purposes of this paper, "scenes" encompass single targets on a GEO background with stars rather than full mega-pixel images; further discussion follows in Section 5. The performance of the overall simulation loop is then used to inform the effects of the optical architecture design trades and can provide insight into the peculiarities of HSI specifically within the SDA GEO design space.

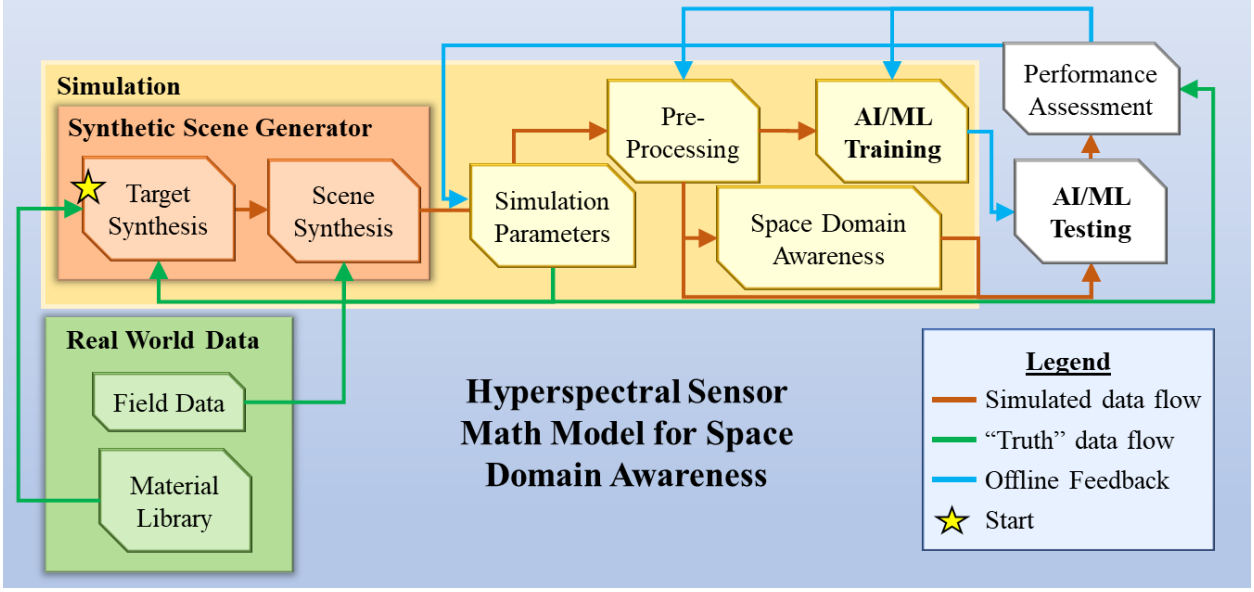

Fig. 2. HSI Simulation Math Model Block Diagram Flow

Real-world data includes both material spectra and field data from sample architectures used to inform the validity of the synthetic scenes and targets from the SSG. These were obtained in-lab by NGC and from subcontractors and are out of the scope of this paper. The following sections discuss the simulation model further in detail.

4. SYNTHETIC SCENE GENERATOR (SSG)

The synthetic scene generator (SSG) uses first principles to simulate everything from photons emitted by the scene to relevant detector counts produced by the focal plane in order to build scenes containing characteristics of interest. Collectively, the input parameters represent the "truth" of the simulated scene, while the realized focal plane readout, including quantization and noise, captures the "measured" scene. An overview of the synthetic scene generator is shown in Fig. 3, where blue boxes are target parameters, purple are sensor parameters, and green are external factors. This model is iterated over spatial dimensions, spectral frequencies, time for temporal dynamics, for each sensor when multiple cameras are used, and for each object (stars, targets, stray light, etc.) to build the simulated scenes. The SSG aims to mimic real data as closely as possible through these multidimensional dynamics as well as using lab measurements to approximate coefficients from target and sensor hardware dynamics.

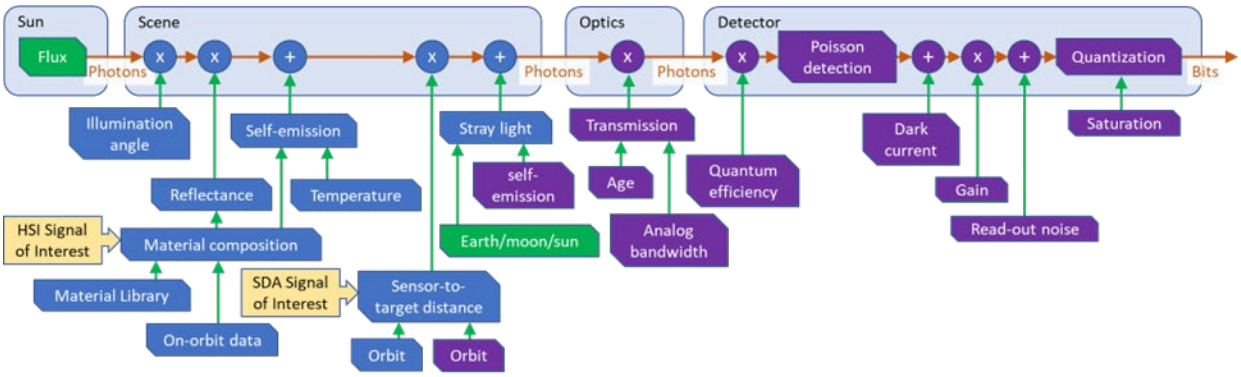

Fig. 3. Synthetic Scene Generator Architecture

The baseline SSG was developed with a finite but extensible architecture. It has been enhanced with new functionality as driven by customer needs, for example the implementation of multiple front-end architectures to optimize the system performance based on orbital regime (e.g. LEO, GEO). The existing model pre-supposes a self-queuing CONOPs; for end-to-end performance modelling, orbital dynamics of the sensor and target are required. These include targets with a variety of lighting conditions, topologies and time-varying target light curves in addition to the

fully illuminated spherical targets currently explored. Gimbal jitter has also been assumed to be negligible at closer ranges, but greater distance-to-target scenarios will necessitate a greater focus in this area in addition to implementing slew rates that impact Field of Regard (FOR) revisit times.

5. PRE-PROCESSING ALGORITHMS

The output of the SSG is configurable from roughly 20x20 pixel snippets around the target of interest, up to full mega-pixel scenes encompassing many targets upon a background containing stars and other sensor artifacts (imitating a collect from a real-world operational system) selectable based on simulation run time and data volume (Fig. 4). Targets are then extracted by pre-processing algorithms for individual analysis via HSI. For the purposes of this paper, these algorithms are considered out of scope and the capability for extracting single targets is assumed. NGC has separate research projects for the development of these algorithms. Thus, a simplification is made to generate only scene "snippets" and the SSG outputs a "one frame centroid" in panchromatic view centered on a ~100-1000 pixel background containing stars (Fig. 5). This image is then "smeared" out spectrally to obtain the hyperspectrum. Raw HSI data represents spectra from (images of) targets of different categories (*e.g.* satellite, space debris, stars) and can be interpreted as a spectral signature. This suggests that **(1)** objects within the same category should ideally be spectrally similar, and **(2)** for adequate classification to occur, objects of different categories should be spectrally different from one another.

These two objectives are not straightforward for SDA applications due to the many variables in target orbital dynamics as well as sensor dynamics which significantly affect how a single object appears on an image spectrum. Pre-processing algorithms spatially, spectrally, and temporarily harmonize the raw focal plane data set to compensate for known distortions. The outputs from this processing are target signatures that are nominally invariant to sensor dynamics (*e.g.* lens vignetting, focal plane temperature, star clutter), which aids in accomplishing **(1)**. Pre-processing is performed on all focal plane data (e.g. in the case of multiple cameras within the sensor) on-orbit within the objective system sensor.

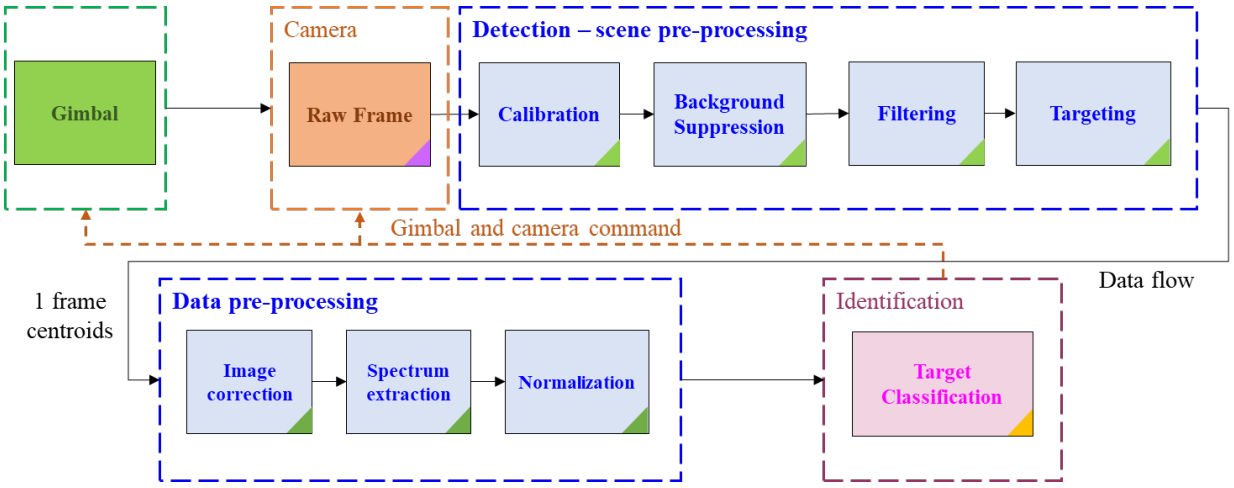

Fig. 4. Data Pre-Processing Flow

Adequate classification, **(2),** is a scientific result of the data, *i.e.* a question of if there is a significant difference between the spectra of different classes of objects under a specified set of conditions, and if it is possible for a hardware imaging system to capture said difference. Classification, **(2),** cannot be the direct result of software processing, which would instead lead to confirmation bias and overfitting.

6. DEEP LEARNING CLASSIFIER

Scene based image classification is a well-studied problem with a vast library of algorithms accomplishing drastically different tasks. To narrow down the initial scope of work, the scene classification problem can first be constrained to identifying single targets, which themselves are preprocessed out of larger scenes into a normalized format for the classifier. These single targets can then be identified through binary classification, *e.g.* as a target that is spoofing

(abnormal) or not spoofing (normal), or through multi-class classification, *e.g.* as a target whose country of origin can be determined from a pool of several countries. In either case, target images are used as a labeled dataset to be passed in as inputs to a machine learning classifier, which then outputs a trained model that can predict the most likely class or classes that an unknown data point belongs to.

Traditional methods for object classification have included k-nearest neighbors (analogous to spectral angle), support vector machines, post classification comparison, normalized difference vegetation index, and decision trees [17-20]. These methods have historically reached an overall classification accuracy of over 90% for binary classification problems, such as identifying vegetation versus non vegetation ground. However, for multi-class classification on hyperspectral data, a typical accuracy is only 60-70%, which necessitates the use of more mathematically complex neural networks [17-20]. Deep learning literature has reported ground-based hyperspectral data yielding accuracies of even >95% given large enough datasets (*i.e.* >100,000 data points) [17-20]. The success of deep learning for hyperspectral classification on ground data motivates this paper's use for space targets.

In GEO, the low spatial resolution of collected images results in a single object being unresolved and spread over only a few spatial pixels due to blur. As such, the spatial information about any target of interest is lost and typical algorithms that learn from image contours or shapes are less effective. Thus, one dimensional (1D) neural networks are used to analyze pooled targets (*i.e.* integrating the point spread function into a single pixel) in spectral domain as separate 1D spectral vectors. The lack of spatial information compared to ground-based applications also results in lower accuracies, which must be compensated for by increasing the size of the training dataset. While this would be challenging on the low volume of real-world data available, the capability for the SSG to generate synthetic data somewhat alleviates this issue. After training the 1D network, performance assessment is performed on a separate set of testing data (*i.e.* data whose labels are known but were not used in the training set). This trained classifier determines the most likely class an unknown object belongs to as well as likelihood scores for all other classes. In other words, a confidence level for each class can be determined for a single unknown object with the sum of all confidence levels equaling 100%. From these, the class with the highest confidence level can be used to identify the unknown object.

7. MATH MODEL OUTPUT

In this paper, the math model is used to generate realistic GEO scenes on varying targets and train a deep learning classifier to output a classification accuracy. Results are then analyzed based this singular system metric (*i.e.* the classification performance). However, in a real-world scenario, additional practical-use parameters such as revisit rate, field of view, and spatial resolution would also be necessary metrics for consideration. The design trades presented this paper are not intended to comprehensively address all of these metrics, but instead aim to demonstrate *how* modeling system architectural design enables their assessment. The classification accuracy is thus provided as an (important) example benchmark, with this then extensible to the other aforementioned metrics as desired.

Performance assessment for the overall design trade should also be viewed in context of the end-to-end math model being a versatile tool for system analysis. One method of evaluation is using the direct classification accuracy to examine how tuning optical architectural parameters either improves or degrades the system accuracy (or other target metric of interest). In this case, this represents the analogy to examining the effects of a hardware design trade on the system performance. Another way to use the math model for system evaluation is *not* using the direct classification accuracy, but rather evaluating the distance at which the accuracy remains above a target threshold (*e.g.* >95% from literature). Since material spectra are deterministic in the absence of noise, it follows that 100% accuracy is expected and has been observed from classification at close distances where noise is much smaller than the object's intensity. The distance at which noise begins to dominate over the object spectrum resulting in a drop in accuracy determines the maximum viewing distance for reasonably confident information extraction. In other words, holding a given system architecture fixed, the performance limit of said system can be examined. A demonstration of how both of these types of assessment can be accomplished is discussed in detail in the following section.

8. RESULTS AND DISCUSSION

This section describes intermediate results and overall performance of the simulation and assessment portions of Fig. 2. The first step was generation of synthetic scenes from the SSG. Sample panchromatic scenes were first generated as shown in Fig. 5 (left). As aforementioned, these were images of single targets centered on the scene with valid targeting and centering algorithms assumed (and out of scope of this paper). The panchromatic scene was then smeared into a mixed spatial and spectral domain (Fig. 5 right) containing the hyperspectrum of the target. Since the target is assumed to be centered on the image in this simulation (see section 5), extraction of only the target's spectrum is straightforward for further processing.

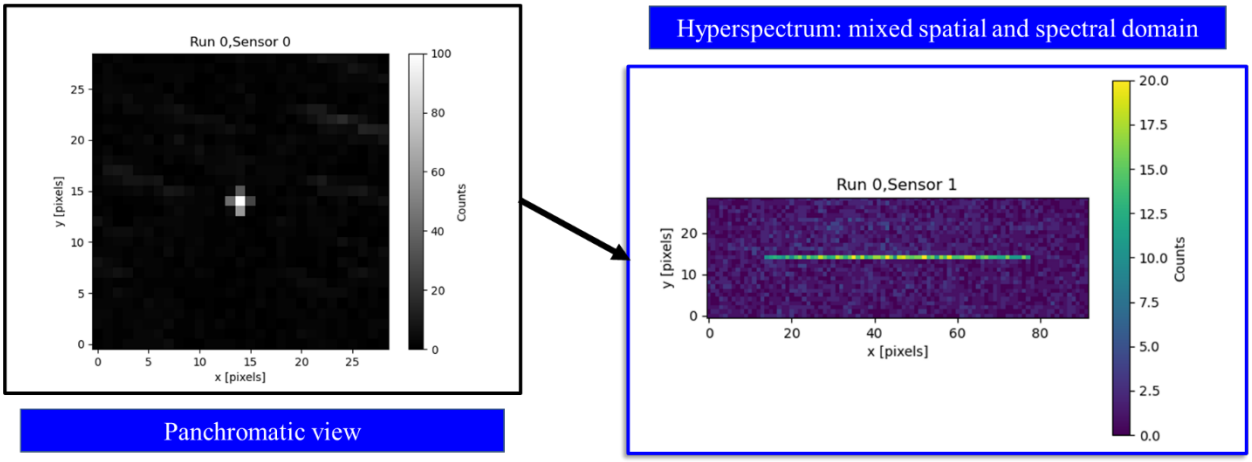

Fig. 5. Synthetic Scene Example

Design trades were evaluated based on several tunable parameters in the SSG, as shown in Table 1. These were used within the optical architecture model to simulate various hardware designs. Data from each combination of cases could then be used for further processing by the AI/ML classifier. Not all parameters were varied in this simulation, but some are still provided as examples of probable areas for further future trade studies. For example, constant optical solar phase angle for illumination is unlikely to be realistic but was used as a basis for initial data simulation. Unless otherwise specified, the number of data points used in each design trade study was 410.

Table 1. Scene Generator Design Trades

Scope	Parameter	Cases			
Target	Model	Spherical			
	Albedo	0.2		0.8	
	Diameter	< 5 meters			
	Distance to sensor (km)	1,000	16,000 (A)	32,000 (B)	64,000 (C)
	Illumination	Optimal solar phase angle			
	Material	Grayscale		Types 1 to 5	
Sensor	Architecture	Visible panchromatic, visible HSI			
Optics (VIS & HSI)	Aperture diameter (mm)	100 (A)		400 (B)	
Focal Plane (VIS & HSI)	Passband	Visible			
	HSI spectral bins	16 (A)	64 (B)		256 (C)
Database	# training data	410 (A)	819 (B)		4096 (C)

An initial analysis was performed on low and high albedo targets with a "grayscale" or uniformly reflecting material. After data generation from the SSG, pre-processing was done to feed the data into the AI/ML classifier. Low (0.2)

and high (0.8) albedo targets were analyzed at a "far" distance of 64,000 km and "small" aperture of 100 mm with varying spectral bins. Classification accuracies—in this case a simple binary classification between low and high albedo—were assessed for each variation in spectral bins. The accuracy can either be reported as an overall accuracy (OA), meaning the number of correctly classified targets divided by the total number of targets, or an average accuracy (AA), meaning the same as overall accuracy but separated by each class and subsequently averaged for the final value. Both are reported in Table 2 for targets with different albedo. All accuracies are given as averages over three different training iterations.

Table 2. Classification accuracies on targets with different albedo

Distance (km)	Aperture (mm)	Bins	OA	AA
64,000 (C)	100 (A)	16 (A)	>99%	>99%
64,000 (C)	100 (A)	64 (B)	>99%	>99%
64,000 (C)	100 (A)	256 (C)	>99%	>99%

Table 2 demonstrates high accuracy no matter the number of spectral bins. This shows that even the most photon starved configuration from Table 1 (far distance, small aperture, and many bins) can achieve high accuracy in a simplified classification problem without any spectral content information. Thus, any drop in accuracy in further simulations when analyzing materials would be a byproduct of the spectral data, not from the classification algorithm or optical architecture.

For further experiments, lab measurements of five different material spectra were obtained using a spectrum analyzer (Fig. 6). These spectra allowed for SSG generation of synthetic scenes containing targets of each of these materials. The purpose was not to obtain highly accurate spectra for detailed scientific hyperspectral analysis on the corresponding materials, but rather to provide a litmus test for demonstrating how well deep learning could distinguish various (unspecified) spectra under a given set of operating conditions. The more rigorous analysis of specific materials is also of interest, but more useful when design trades are more advanced to allow for building of hardware systems capable of probing specific applications.

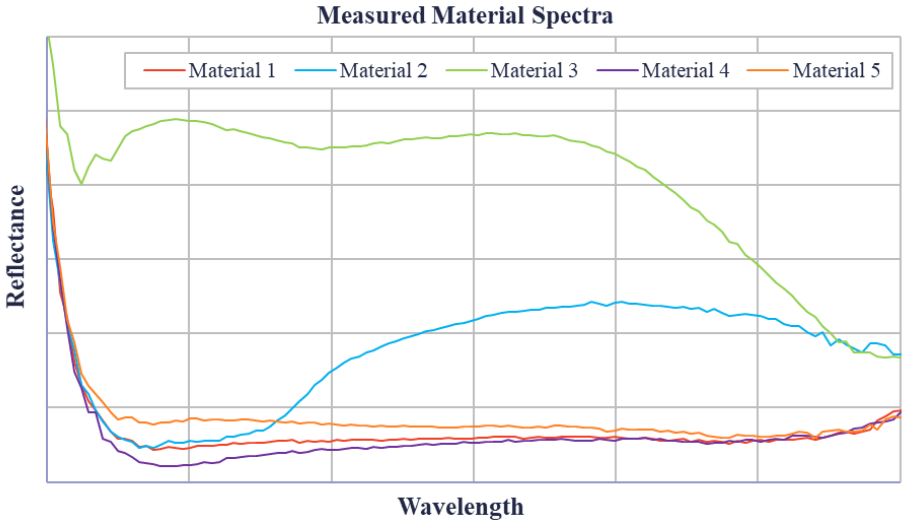

Fig. 6. Lab Spectrum Analyzer Measured Material Spectra

The spectra in Fig. 6 provide a variety of test cases for classification analysis. While the spectra for materials 2 and 3 are fairly distinct, the reflectances for materials 1, 4, and 5 are all similar and low across the wavelengths of interest.

Both the distinctness and the absolute reflectivity of analyzed spectra are likely to play differing roles in system accuracy over the design trades listed in Table 1. These are detailed in the following results. First, another base case was examined where the materials were assessed at a "control" distance of 1,000 km, *i.e.* a very close distance at which all spectral bins were calculated to be above background noise (using aperture A, bins B). The results are provided in Table 3, demonstrating that near perfect accuracy can be achieved for classifying single materials with a sufficient signal-to-noise ratio relative to background. In other words, this control shows that deep learning algorithms can distinguish between different materials based on the differences in their hyperspectra.

Table 3. Classification accuracies on 5 different materials at control distance

	Accuracy
OA	>99%
AA	>99%
Material 1	>99%
Material 2	>99%
Material 3	>99%
Material 4	>99%
Material 5	>99%

The first two studies were base cases aimed at demonstrating the possibility for deep learning algorithms to accurately classify hyperspectral space target data. With these having shown that high accuracy information extraction is possible under ideal conditions (*e.g.* close distance or simplistic spectra), more realistic conditions were then examined. First, distances (A) and (B) were assessed for classification of the 5 different materials (at aperture A, bins B). The results are reported in Table 4 including the per class accuracy. While both OA and AA drop drastically for both distances A and B, the drop in accuracy was lower for aterials 2 and 3 than for the other 3 materials. In order to assess why this might be the case, the percentage of bins over a signal-to-noise-ratio (SNR) of 2 were evaluated for each material and reported in Table 5. In this case, the signal was calculated as the average bin signal strength, while the noise was calculated as standard deviation of background noise.

Table 4. Classification accuracies on 5 different materials at realistic (close – A, medium – B) distances

Distance (km)	OA	AA	Material 1	Material 2	Material 3	Material 4	Material 5
16,000 (A)	71%	71%	40%	99%	>99%	58%	62%
32,000 (B)	52%	54%	32%	79%	90%	37%	33%

Table 5. Percentage of bins over 2 SNR for 5 different materials at realistic (close – A, medium – B) distances

Distance (km)	Material 1	Material 2	Material 3	Material 4	Material 5
16,000 (A)	20%	84%	97%	6%	67%
32,000 (B)	2%	13%	81%	2%	2%

At each distance, Table 5 suggests that the higher accuracies associated with materials 2 and 3 are associated with the larger percentage of bins above the noise level. However, combined analysis with Table 4 shows that material 2 at distance B demonstrates an 79% classification accuracy with only 13% bins above the noise level, while materials 1 and 5 at distance A show lower accuracies at 40% and 62% despite having respectively larger percentages (20% and 67%) of bins above the noise level. In other words, the percentage of bins above the noise level was not the only predictor of classification accuracy, but other factors like the degree of spectral relatedness (*i.e.* spectral angle between materials) also affect performance (Fig. 6). In this case, both the low reflectance and high spectral similarity of materials 1, 4, and 5 likely play a role in their low accuracy at a close distance A, where it is not immediately clear from the SNR why this might be the case.

This observation demonstrates the complexity behind system outputs and how performance metric outcomes are difficult to determine based on simple variables like SNR. Many factors, varying over a myriad of different applications with different data inputs, are involved to allow for the extraction of useful information from target hyperspctra. Therefore, this math model pipeline from scene simulation to analysis provides a way to assess the effects of design trades on performance outcomes without the need for complicated and detailed analysis of confounding intermediate variables. In this example, tables 4 and 5 suggest that decreasing the distance is not enough to drastically improve the accuracy on spectrally similar materials and that tuning optical architectural parameters may be necessary. Thus in the following experiment, the aperture size and number of spectral bins were varied in Table 6 (at distance A) and accuracies re-examined against distance A (aperture A, bins B) as the base case. This represents an example of an architectural design trade as described in section 7.

Table 6. Classification accuracies on materials varying aperture and number of spectral bins at distance A

Aperture Diameter (mm)	Bins	OA	AA	Material 1	Material 2	Material 3	Material 4	Material 5
100 (A)	16 (A)	87%	89%	67%	>99%	>99%	91%	86%
100 (A)	64 (B)	71%	71%	40%	99%	>99%	58%	62%
100 (A)	256 (C)	71%	71%	41%	>99%	>99%	58%	56%
400 (B)	16 (A)	95%	96%	85%	99%	>99%	98%	97%
400 (B)	64 (B)	97%	97%	90%	>99%	>99%	98%	98%
400 (B)	256 (C)	96%	97%	89%	>99%	>99%	98%	98%

Table 6 shows that increasing the number of bins interestingly has minimal effect on OA and AA when aperture is small, while decreasing the number of bins improves the accuracy. The same is not true for the larger aperture with increased photon throughput, where a by material analysis shows improved performance in material 1 as bins are increased from 16 (case A). This shows how one design trade along a given dimension (aperture) can affect the choice

of other architectural choices, in this case the number of bins. Under these given conditions, the larger aperture clearly offers a large improvement in classification accuracy at the usual drawback of being more expensive. Then given the larger aperture, this design trade suggests that using more hyperspectral bins for "close" distance (A) imaging would be beneficial. For further distances, this trade on number of bins (at the larger aperture, B) was again analyzed in Table 7.

Table 7. Classification accuracies on materials varying distance and number of spectral bins at aperture B

Distance (km)	Bins	OA	AA	Materia l 1	Material 2	Material 3	Material 4	Material 5
16,000 (A)	16 (A)	95%	96%	85%	99%	>99%	98%	97%
16,000 (A)	64 (B)	97%	97%	90%	>99%	>99%	98%	98%
16,000 (A)	256 (C)	96%	97%	89%	>99%	>99%	98%	97%
32,000 (B)	16 (A)	82%	82%	62%	96%	>99%	75%	75%
32,000 (B)	64 (B)	81%	83%	59%	>99%	99%	77%	78%
32,000 (B)	256 (C)	81%	82%	50%	>99%	>99%	84%	84%
64,000 (C)	16 (A)	60%	61%	35%	75%	95%	49%	48%
64,000 (C)	64 (B)	61%	62%	37%	92%	95%	42%	42%
64,000 (C)	256 (C)	64%	63%	35%	98%	97%	41%	46%

Table 7 shows that accuracy is predictably degraded as distance increases, from 95-97% at close distances (A) to 60-64% at far distances (C). In this case, the optical architecture is fixed, and the simulation used as a way to assess the limits of the overall system performance (the second type of assessment described in section 7). In other words, the maximum operating distance of this architecture (aperture B with a chosen number of bins) to maintain a high confidence level of 95% would be the "close" distance of 16,000 km (case A). Farther distances provide less fidelity of information but could also be considered for applications where lower accuracy can be tolerated.

Interestingly, table 7 shows that increasing the number of bins at each distance does not reduce the accuracy. This could be due to several factors: it could be that the SNR of a select few critical bins is the key factor in differentiating between materials, or that the increase in spectral content information is enough to offset the reduction in SNR with more bins. The point of this experiment is again not to elucidate the details of how the 5 particular materials in this study can be spectrally identified, but rather to demonstrate how this math model provides a framework for examining the effects of design trades under different conditions of interest (in this case distance). From here, scientific information about a specified problem (*e.g.* determining what allows for spectral identification of a set of materials) under the simulated conditions could be determined via detailed analysis of intermediate variables, like intensity or reflectivity in specified wavelength bands.

A final study was performed by increasing the amount of data per material class. The accuracy of deep learning algorithms scales with number of training data to allow for more complexity while avoiding overfitting (typically at least 1,000 data points per class for high accuracy). While this volume of real-world data is extremely difficult to obtain due to the low downlink bandwidth and difficulty of accurately obtaining targets, the math model provides an

advantage in being able to facilely simulate this amount of generated data. Increased data volume is assessed in Table 8 at distance B, aperture A, and bins B. Increased classification accuracies are observed, with a roughly ~10% gain in accuracy observed when 10 times the amount of training data is used. Although significant, the high complexity of the SSG still limits the rate at which data can be generated and is thus main limiting factor in the rapid experimentation capabilities of the math model. There is therefore a tradeoff between increased data volume and development time that must be accounted for and the reason for choosing the lower data volume (410, A) for the other experiments. Higher data volumes would potentially be more useful for higher quality assessments in later technical design stages, or for transfer learning to real hardware.

Table 8. Classification accuracies on materials varying data volume

# data per class	OA	AA	Material 1	Material 2	Material 3	Material 4	Material 5
410 (A)	54%	52%	32%	79%	90%	37%	33%
819 (B)	57%	56%	30%	86%	92%	36%	40%
4096 (C)	62%	63%	35%	90%	94%	46%	44%

9. SUMMARY AND FUTURE WORK

This paper detailed the development and usage of a three-part math model simulator for a hyperspectral imager for space domain awareness. Design trades using the math model were examined, revealing the capability for both assessing the effects of optical architectural trades on overall system performance, as well as performance limits for a given system architecture. While classification accuracies under realistic conditions were observed to reach >95%, these experiments were designed to show how the math model can be used as a tool for system design iteration rather than only to achieve the highest accuracy possible. As a software method for exploring the HSI-SDA design space, this math model thus provides a cost effective and rapid way to alleviate the difficulties of developing on-orbit hardware systems.

Given that this math model is only a lab measurement informed software simulation, several priority next steps are to validate and improve the veracity of the model. While many multidimensional dynamics were already incorporated from first principles, implementation of as many phenomena as possible (*e.g.* especially illumination and different model shapes) allows for simulation of scenes that mimic reality as closely as possible. Furthermore, comparison against real-world telescope data would allow for verification of statistically equivalent output to real data, allowing for a greater understanding of instrument operation as well as building confidence in the reliability of the "truth" parameters the math model is built upon.

One target is developing a hardware flatsat in conjunction with the math model. This work aims to obtain samples of the real data necessary to inform and tune the simulation, but also to demonstrate that the baseline capabilities purported by this paper are realistic. An addendum to this is collecting additional material samples using said flatsat, improving the diversity and quality of spectral data for analysis via deep learning. From here, semi-realistic scenes can be taken to supplement the simulated data, or as testing data for transfer learning using the math model detailed in this paper.

10. REFERENCES

[1] Hu, Y. P.; Li, K.; Liang, Y. G.; Chen L. *Review on strategies of space-based optical space situational awareness* **Journal of Systems Engineering and Electronics**, vol. 32 no. 5, 1152-1166, 2021.
[2] Bingen, K. A.; Johnson, K.; Young, M.; Raymond, J. W. *Space Threat Assessment 2023* **Center for Strategic and International Studies.**

[3] Wang, B. C.; Li, S.; Mu, J. Z.; Hao, X.; Zhu, W. S.; Hu, J. Q. *Research Advancements in Key Technologies for Space-Based Situational Awareness* **Space: Science and Technology**, vol. 2022.
[4] Kennewell, J. A.; Vo, B. N. *An Overview of Space Situational Awareness* **2013 16th International Conference on Information Fusion**, 1029-1036, 2013.
[5] Tanaka, K. *Applicability of Remote Sensing Policies to Space Situational Awareness* **Space Policy**, vol. 42, 83-91, 2017.
[6] van der Meer, F. D.; vander Werff, H. M. A.; van Ruitenbeek, F. J. A.; Hecker, C. A.; Bakker, W. H.; Noomen, M. F.; van der Meijde, M.; Carranza, E. J. M.; de Smeth, J. B.; Woldai, T. *Multi- and Hyperspectral Geologic Remote Sensing: A Review* **International Journal of Applied Earth Observation and Geoinformation,** vol. 14, 112-128, 2012.
[7] Adao, T.; Hruska, J.; Padua, L.; Bessa, J.; Peres, E.; Morais, R.; Sousa, J. J. *Hyperspectral Imaging: A Review on UAV-Based Sensors, Data Processing, and Applications for Agriculture and Forestry* **Remote Sensing**, vol. 9, 2017.
[8] Loncan, L.; Almeida, L. B.; Bioucas-Dias, J. M.; Briottet, X.; Chanussot, J.; Dobigeon, N.; Fabre, S.; Liao, W. Z.; Licciardi, G. A.; Simoes, M.; Tourneret, J. Y.; Veganzones, M. A.; Vivone, G.; Wei, Q.; Yokoya, N. *Hyperspectral Pansharpening: A Review* **IEEE Geoscience and Remote Sensing Magazine**, Vol. 3, 27-46, 2015.
[9] Qian, S. E. *Hyperspectral Satellites, Evolution, and Development History* **IEEE Journal of Selected Topics in Applied Earth Observations and Remote Sensing**, vol. 14, 7032-7056, 2021.
[10] Zeng, L. L.; Wardlow, B. D.; Xiang, D. X.; Hu, S.; Li, D. R. *A Review of Vegetation Phenological Metrics Extraction using Time-Series, Multispectral Satellite Data* **Remote Sensing of Environment**, vol. 237, 2020.
[11] Lu. B.; Dao, P. D.; Liu, J. G.; He, Y. H.; Shang, J. L. *Recent Advances of Hyperspectral Imaging Technology and Applications in Agriculture* **Remote Sensing**, vol. 12, 2020.
[12] Dozier, J.; Painter, T. H. *Multispectral and Hyperspectral Remote Sensing of Alpine Snow Properties* **Annual Review of Earth and Planetary Sciences**, vol. 32, 465-494, 2004.
[13] Transon, J.; d'Andrìmont, R.; Maugnard, A.; Defourny, P. *Survey of Hyperspectral Earth Observation Applications from Space in the Sentinel-2 Context* **Remote Sensing**, vol. 10, 2018.
[14] Phiri, D.; Simwanda, M.; Salekin, S.; Nyìrenda, V. R.; Murayama, Y.; Ranagalage, M. *Sentinel-2 Data for Land Cover/Use Mapping: A Review* **Remote Sensing**, vol. 12, 2020.
[15] Eisfelder, C. Kuenzer, C.; Dech, S. *Derivation of Biomass Information for Semi-Arid Areas using Remote-Sensing Data* **International Journal of Remote Sensing**, vol. 33, 2937-2984, 2012.
[16] Asadzadeh, S.; de Souza, C. R. *A Review on Spectral Processing Methods for Geological Remote Sensing* **International Journal of Applied Earth Observation and Geoinformation**, vol. 47, 69-90, 2016.
[17] Shi, W. Z.; Zhang, M.; Zhang, R.; Chenf, S. X.; Zhan, Z. *Change Detection Based on Artificial Intelligence: State-of-the-Art and Challenges* **Remote Sensing**, vol. 12, 2020.
[18] Tsouros, D. C.; Bibi, S.; Sarigiannidis, P. G. *A Review on UAV-Based Applications for Precision Agriculture* **Information**, vol 10, 2019.
[19] Lawrence, R. L.; Moran, C. J. *The AmericaView Classification Methods Accuracy Comparison Project: A Rigorous Approach for Model Selection* **Remote Sensing of Environment**, vol. 170, 115-120, 2015.
[20] Audebert, N.; Saux, B.; Lefèvre, S. *Deep Learning for Classification of Hyperspectral Data: A Comparative Review* **IEEE Geoscience and Remote Sensing Magazine**, vol. 7, 159-173, 2019.